CHEMISTRY OF MATERIALS

ARTICLE

pubs.acs.org/cm

Synthesis of Single Crystal Hollow Silver Nanoparticles in a Fast Reaction-Diffusion Process

Assaf Ben Moshe and Gil Markovich*

School of Chemistry, Beverly and Raymond Sackler Faculty of Exact Sciences, Tel Aviv University, Tel Aviv 69978, Israel

Supporting Information

ABSTRACT: Colloidal hollow silver nanoparticles were produced by a fast chemical reduction of silver oxide nanoparticles capped with glutathione. These hollow silver particles were surprisingly single crystalline and had almost perfect spherical shells. The reaction was further tested for the transformation of silver oxide nanoparticles to hollow silver sulfide nanoparticles by a reaction with sulfide ions. Analysis of the dimensions of the precursor Ag_2O nanoparticles and product hollow Ag nanoparticles as well as the sensitivity of the reduction process to the nature of reducing agent and its concentration hints that the reaction had to proceed through inward diffusion of reducing agent versus fast outward diffusion/dissolution of silver ions. We believe that this type of reactions resembles transformation reactions that have been associated with the nanoscale Kirkendall effect in its broader sense.

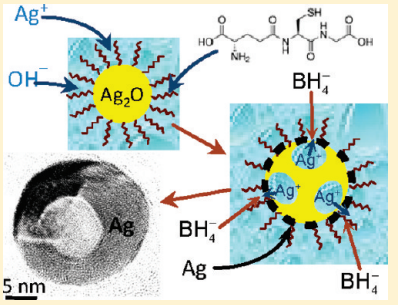

KEYWORDS: nanomaterials, nanoparticles, colloids, crystal growth

INTRODUCTION

The synthesis of hollow metal nanostructures is of interest because of their special, tunable optical properties. Extensive work has been done by Halas and co-workers, following an initial demonstration by Zhow and co-workers,[1] to control the plasmonic properties of dielectric-gold[2] and dielectric-silver[3] core−shell nanoparticles. Since then, this group and few others have shown applications of these particles in different fields of plasmonics and photonics such as surface enhanced Raman scattering (SERS) for molecules adsorbed to the external surface of the shell,[4] and recently SERS for molecules within the shells.[5] Surface enhancement of other optical methods such as Raman optical activity,[6] infrared absorption,[7] fluorescence[8] and two photon fluorescence[9] using hollow metal nanoparticles was also demonstrated. Other applications for hollow metal and dielectric-metal core−shell nanoparticles, in medicine,[10] catalysis,[11] and improved sensing for analytical puposes,[12] were also demonstrated. Hollow metal structures are usually prepared by metal deposition on various spherical templates, usually leading to relatively rough and polycrystalline metal shells.[2b,13] Xia and coworkers have applied the galvanic replacement of metal templates for the synthesis of hollow metal structures.[14] In addition, there are very few demonstrations of synthesis of hollow metal structures, and specifically hollow silver nanostructures, through the conversion of reactive templates. The most common and efficient conversion of reactive templates for the formation of hollow nanoparticles involves the nanoscale Kirkendall effect. The Kirkendall effect was first observed experimentally in 1942 and then repeated in 1947 for an interface between copper and brass.[15] It is classically described as a process occurring at the interface of two components where a mutual counter diffusion at different rates forces diffusion of vacancies to compensate for inequality in the material flow.[16] The accumulation of the vacancies forms the hollow interior. Its first demonstration at the nanoscale by Alivisatos and co-workers in 2004 has attracted a great deal of interest.[17] Their preparations of hollow cobalt oxide and chalcogenide nanoparticles have proceeded through a mechanism very similar to the bulk Kirkendall effect, with some unique features of nanoscale reactions. Since then, a variety of hollow morphologies of many different inorganic materials were synthesized via this or related effects, addressed as the nanoscale Kirkendall effect in a broader sense.[18] More specifically Yang et al. have demonstrated the synthesis of hollow rhombododecahedral silver microstructures by reduction of silver phosphate or silver oxide microcrystals with different reducing agents.[19] In this case the authors suggested that this reaction proceeded through the microscale Kirkendall effect, described as a coupled reaction-diffusion process, a term that was previously mentioned in connection with this effect.[17] The reaction resulted in polycrystalline shells that were formed by the morphology preserving alignment of the formed silver clusters. Another recent work, which is relevant to the case presented here, is the synthesis of hollow cubic cobalt nanoparticles via oleylamine reduction of CoO cubic nanoparticles, excluded from the Kirkendall type reactions by the authors.[20] In that work the mechanism proposed involved continuous diffusion of oxide to the surface followed by

Received: October 17, 2010
Revised: December 13, 2010
Published: January 21, 2011

removal as carbon monoxide, while the outer reduced cobalt shell transfers electrons to the inner cobalt ions.

In this paper we report on a reaction-diffusion process at a nanoscale system, which yields hollow metal nanostructures that are not just morphology preserving but are single-crystalline. This is demonstrated by the synthesis of hollow single crystal silver nanospheres by the reduction of silver oxide nanoparticles that are formed in water, and stabilized by glutathione. This process, being strongly kinetically controlled, bears resemblance to the nanoscale Kirkendal effect. The method was further extended to attempt the synthesis of hollow silver sulfide and silver bromide nanostructures for a better understanding of the parameters controlling the formation of the hollow nanospheres. This method offers a unique solution for the synthesis of relatively small hollow silver nanoparticles of 20−40 nm in diameter, while other synthesis methods typically produce hollow metal nanoparticles ∼100 nm in diameter or larger.

MATERIALS AND METHODS

Materials. Silver nitrate (ACS reagent grade), sodium borohydride (puriss. p.a. grade), L-glutathione in reduced form (assay over 98%), sodium citrate dihydrate (99% assay, FG), hydrazine hydrate solution (78−82% assay, acidimetric), sodium-L- ascorbate (99% assay, Bioxtra), sodium sulfide nonahydrate (ACS reagent grade), sodium bromide (purum), and sodium hydroxide (ACS reagent grade) were obtained from Sigma-Aldrich and used without additional purification. Ultrapure water was obtained from a USF ELGA UHQ system.

Synthesis. The silver nanoparticles were synthesized using the following procedure: To 2.6 mL of ice cold water were added aqueous solutions of silver nitrate (150 μL, 10 mM) and glutathione (18 μL, 10 mM) (similar nanoparticles were synthesized using sodium citrate as a surfactant as well, see Supporting Information). The pH of the solution was raised to ∼12 by adding an aqueous solution of sodium hydroxide (500 μL, 0.1M), while vigorously stirring. After the solution had turned pale yellowish, signifying the formation of Ag_2O nanocrystals, a freshly prepared sodium borohydride solution was introduced at once (180 μL, 10 mM). Similarly, the reaction was performed by replacing the borohydride solution with sodium ascorbate solution (aqueous, 50 mM, 500 μL), or hydrazine hydrate solution (aqueous, ∼16.5 mM, 250 μL, prepared by diluting 1 μL ∼80% hydrazine hydrate solution to a final volume of 1 mL with water). The formation of hollow silver sulfide or silver bromide nanoparticles was performed by replacing the reducing agent with aqueous solutions of sodium sulfide (75 μL, 10 mM) or sodium bromide (150 μL, 10 mM).

Ag samples for experiments with partial reduction were prepared as described above, with the exception that only 0.9 and 27 μL of sodium borohydride solution were introduced.

X-ray diffraction (XRD) data was collected with Cu K_α radiation on Θ−Θ powder diffractometer "Scintag" equipped with a liquid nitrogen cooled Ge solid-state detector.

Absorption Measurements. Steady state absorption measurements were performed in a Cary 5000 UV−vis-NIR spectrophotometer. Silver nanocapsule solution was diluted ×3 in an aqueous solution of sodium hydroxide (pH 12). The absorption spectrum of the silver oxide nanoparticles solution was measured without dilution. The absorption spectrum evolution at the first seconds of the reduction reaction was probed with an Ocean Optics S2000 spectrometer with the cuvette holder mounted on a magnetic stirrer. The spectra were acquired with 10 ms integration time, and the sampling rate was ∼100 Hz.

Electron Microscopy. Transmission electron microscopy (TEM) images were recorded using an FEI Tecnai F20 FEG-TEM. All samples for TEM imaging were deposited on carbon coated 300-mesh Cu grids obtained from SPI. Scanning electron microscopy (SEM) images were recorded using a Quanta 200 FEG environmental SEM, operating at high vacuum mode. All samples for SEM were deposited on Holey carbon coated 300 Mesh cu grids obtained from SPI. Images were taken in a 20 degrees tilt.

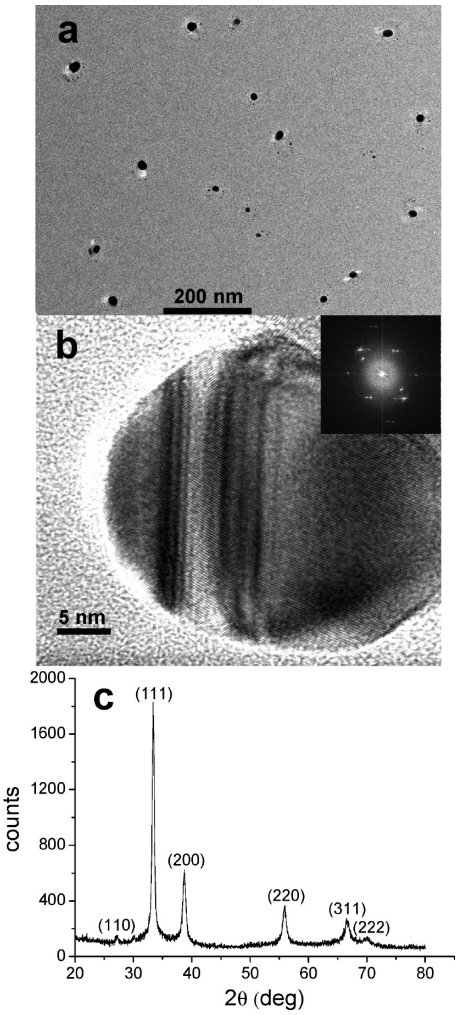

Figure 1. (a) Low magnification TEM image of the Ag_2O nanocrystals serving as precursors for the preparation of the Ag nanocapsules. (b) High resolution TEM image with corresponding Fourier transform of a single Ag_2O nanocrystal. (c) XRD pattern of the dried Ag_2O nanocrystal solid. The pattern fits Ag_2O well, and line width analysis yielded a grain size of ∼25 nm.

RESULTS AND DISCUSSION

The preparation of the hollow silver nanoparticles starts with the preparation of silver oxide nanoparticles by precipitating silver ions in a highly basic solution in the presence of glutathione as a capping molecule. Figure 1 displays a TEM image (Figure 1a), a high resolution TEM image (Figure 1b), and an XRD pattern (Figure 1c) of the template silver oxide nanoparticles. According to the XRD line width analysis the average nanoparticle size was ∼25 nm, which is in rough agreement with the TEM images. The XRD pattern fits bulk Ag_2O data. High resolution TEM images such as the one presented show that the template silver oxide nanoparticles were mostly single crystalline, this fact is important since it appears that the nature of the resulting hollow silver nanoparticles depends on that of the

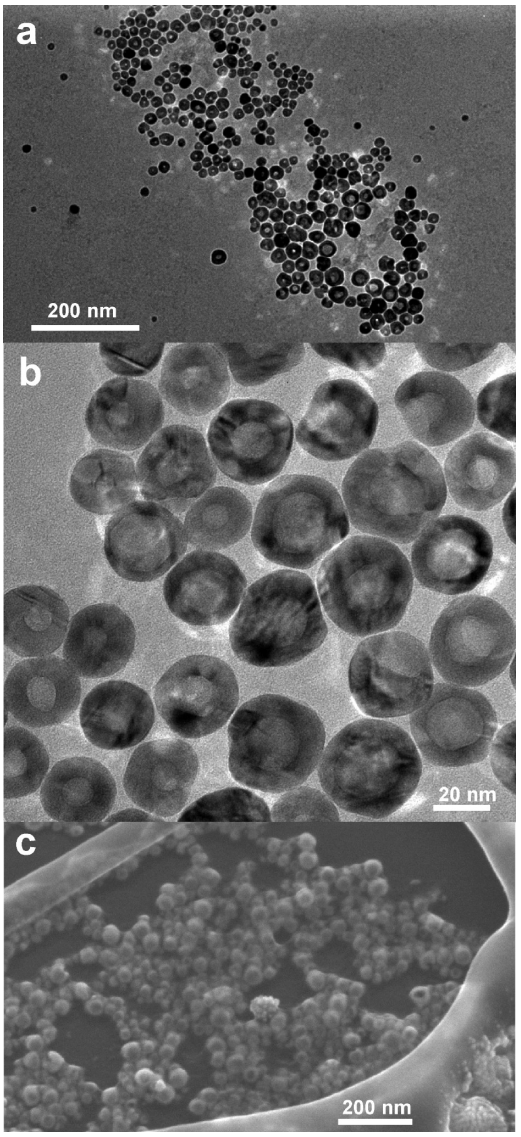

Figure 2. (**a, b**) TEM images of hollow silver nanoparticles formed immediately after the addition of the reducing agent, at two different magnifications. (**c**) SEM image of the same particles.

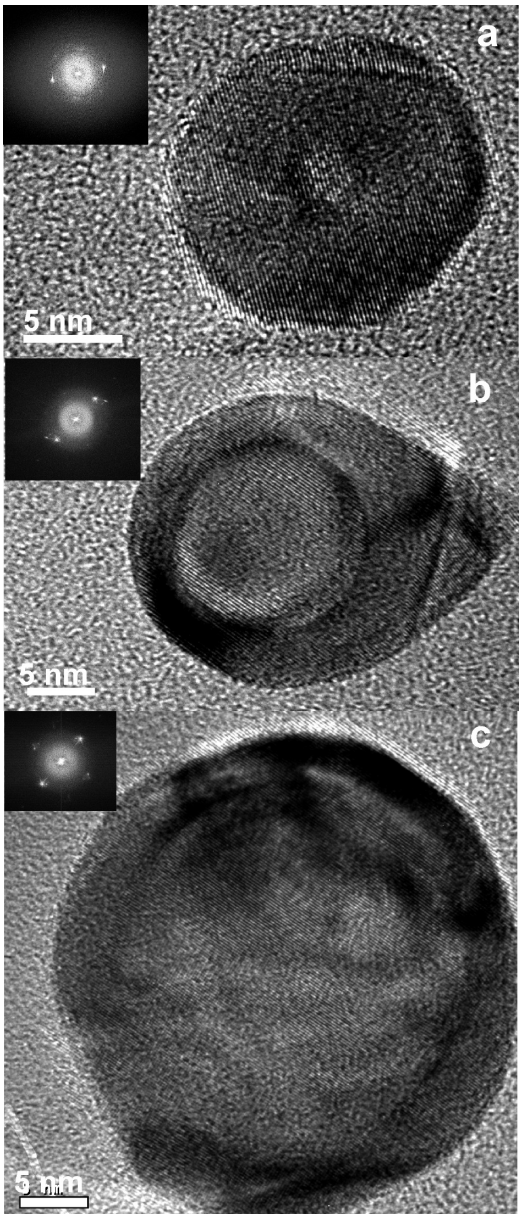

Figure 3. (**a,b,c**) HRTEM images of individual hollow nanoparticles along with their Fourier transforms depicting their single crystalline structure. The nanoparticles' relative cavity size increases from **a** to **c**.

reactive template. Similar nanoparticles were successfully synthesized using other surfactants such as sodium citrate (see Supporting Information, Figure S1).

Following the preparation of the Ag_2O nanoparticles, an excess of sodium borohydride was added with vigorous stirring to the nanoparticle solution, and an orange color appeared instantly, indicating the reduction of silver oxide to silver nanoparticles. Figure 2 displays TEM images with two different magnifications (Figure 2a,b) and a high resolution scanning electron micrograph (Figure 2c) of the hollow silver nanoparticles formed after adding the reducing agent to the Ag_2O nanoparticle suspension. Size statistics obtained from about 100 hollow nanoparticles resulted in outer diameters of 27 $\pm$ 7.5 nm and shell thicknesses of 7.3 $\pm$ 1.5 nm. The scanning electron micrograph shows that a small part of the particles have perforated shells, but most of the spheres seem to have symmetric round closed shells. In addition, high resolution TEM images presented in Figure 3, together with their corresponding Fourier transforms, depict the single crystalline nature of the hollow particles of different sizes, with different relative cavity sizes.

A simple calculation based on the silver shell volume of each nanoparticle, the densities of silver and silver oxide, and assuming that all the silver oxide was converted to silver can give an estimate of the volume of the original silver oxide nanoparticle (see Supporting Information for details). It was found that the outer diameter of the hollow nanoparticle was usually about the same or slightly smaller than the calculated diameter of the template Ag_2O nanoparticle. This indicates that the reaction had to involve inward diffusion of the reducing agent, or of electrons injected by the reducing agent at the metal surface. The reaction front location would depend on the difference between the rates of reducing agent inward diffusion and silver ions outward diffusion. Individual cases where the estimated precursor Ag_2O

dx.doi.org/10.1021/cm102991z |*Chem. Mater.* 2011, 23, 1239–1245

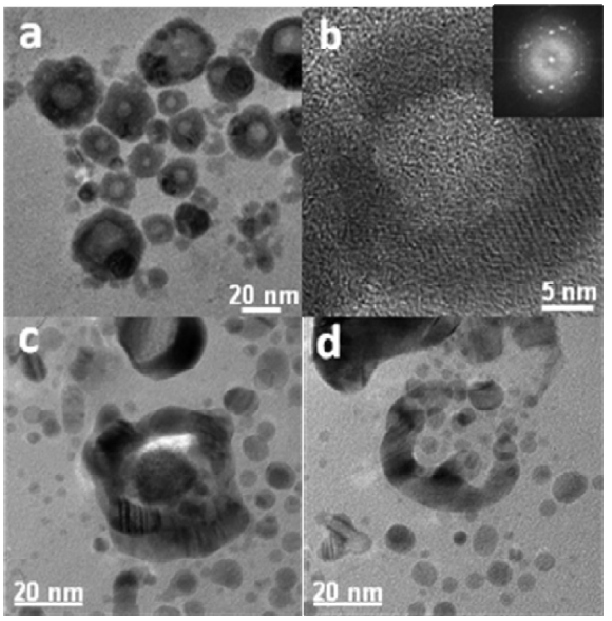

Figure 4. (**a**) TEM image of hollow Ag_2S nanoparticles formed after addition of sulfide ions. (**b**) A high resolution image of one of the Ag_2S particles presented with its Fourier transform, indicating the polycrystalline nature of these nanoparticles. (**c,d**) Typical images of AgBr nanoparticles formed after the addition of bromide ions.

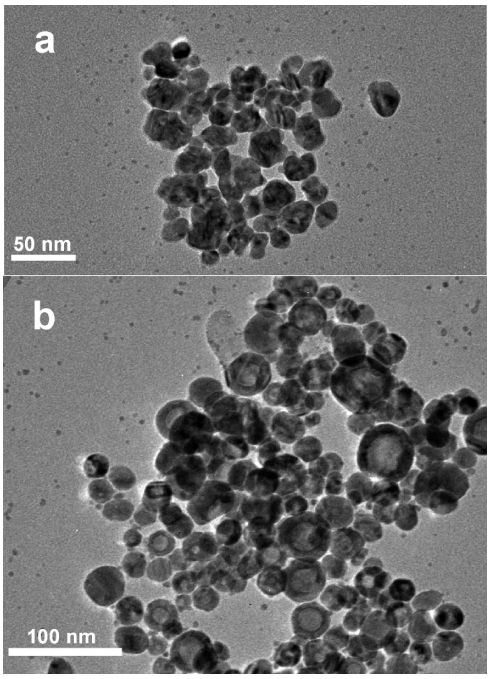

Figure 5. TEM images of Ag_2O nanoparticles transformed to Ag nanostructures by alternative reducing agents: (**a**) sodium ascorbate and (**b**) hydrazine.

particle diameter was somewhat larger than the hollow Ag nanoparticle diameter were probably due to larger amounts of unreacted silver oxide left in the core of the particle. This is supported by XPS measurements on the hollow Ag nanoparticles, indicating that residual silver oxide remained in an amount which is much larger than expected of a thin oxide layer at the outer surface of the particles, see Supporting Information, Figure S2. The relative uniformity of shell thickness might suggest that there is a critical thickness of the shells beyond which the reduction stops and that it is not strongly dependent on the original particle size. Consequently, reduction of larger silver oxide nanoparticles would result in the same Ag shell thickness as in small particles but with more remaining silver oxide at the core. An addition of excess amounts of reducing agent to the hollow nanoparticles suspension was monitored by absorption measurements and did not reveal any change, indicating that the shells are impenetrable for reducing agent species and that electron transfer to the inner Ag_2O is inhibited after the end of the shell formation.

The attempted preparation of hollow silver sulfide or silver bromide nanoparticles was performed by replacing the reducing agent with aqueous solutions of sodium sulfide or sodium bromide, respectively. Figure 4 displays TEM images of typical hollow silver sulfide nanoparticles (Figures 4a,b) formed, together with typical images of silver bromide nanoparticles formed by the transformation reaction (Figures 4c,d). The different phases were also verified by selected area electron diffraction (See Supporting Information, Figure S3). The oxide-sulfide transformation led to a high yield of hollow Ag_2S nanoparticles, while the oxide-bromide transformation resulted in a large population of small nanoparticles with a very low yield of defective hollow nanoparticles. The hollow silver sulfide nanoparticles had polycrystalline morphology and more defective shells relative to the hollow Ag nanoparticles.

Another set of experiments was performed to understand the effect of different reducing agents on the process as well as that of temperature. Alternative reducing agents were added at large excess. Figure 5 is a TEM image of nanoparticles formed on reduction with ascorbate (Figure 5a) and hydrazine (Figure 5b). Reaction with ascorbate did not yield hollow morphologies, while reaction with hydrazine yielded hollow morphologies with lower efficiency than sodium borohydride. At micrometer-scale particles, the control of the reducing agent's molecular volume has led to different multishell morphologies through control of its inward diffusion rate.[19] However, the nanoscale transformation reaction was more sensitive to the reducing agent's properties, and the use of other reducing agents interfered with the yield of hollow nanoparticles. This can be explained by either the reduction potential of each reducing agent and their respective electron transfer rates or their inward diffusion rates. Dissolution of silver oxide and outward diffusion of silver ions had to occur very fast, which made it necessary for the reducing agent to diffuse inward very fast to form the perfect shells, or efficiently transfer electrons through the growing Ag shell. The temperature range for efficient synthesis was 0−50 °C. At higher temperatures the hollow particle yield decreased, and above 70 °C the formation of hollow nanoparticles was not observed. This might be explained again by the increasing rate of dissolution of silver oxide and outward diffusion of silver ions to form separated nucleation centers upon reduction which led to formation of regular nanoparticles and aggregates.

When the transformation reactions were performed with the slow, dropwise addition of the reducing agent, or with lower reducing agent concentrations, the silver shells became discontinuous and highly non-uniform, and many small nanoparticles (<10 nm) were observed (see details in the Supporting Information, Figure S4). Attempts to stop the reaction at different stages were performed by partial reduction. Figure 6 displays a TEM

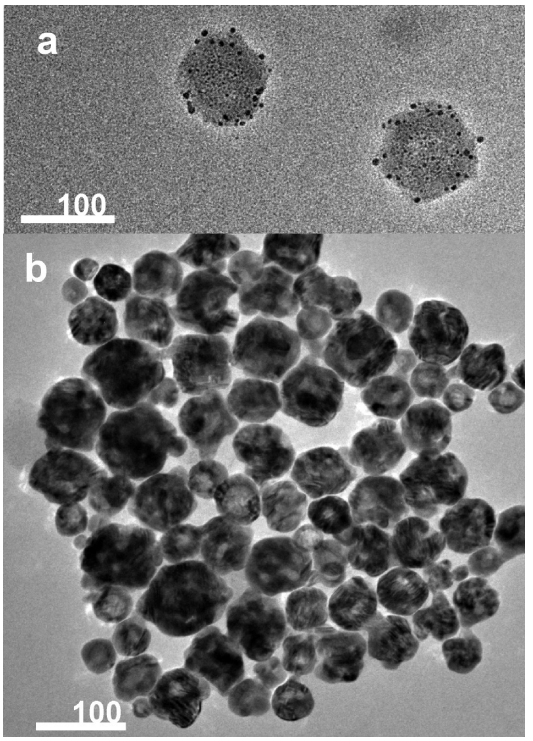

Figure 6. Silver nanoparticles formed after partial reduction with (**a**) 0.5% and (**b**) 15% of the original reducing agent concentration.

image of Ag_2O/Ag nanoparticles formed after addition of 0.5% (Figure 6a), and 15% (Figure.6b) of the reducing agent concentration used in the original transformation reactions. However, these images probably do not reflect the exact progress of the fast reduction process, and instead the outcome is controlled by the slower reduction rates. It is clear that for this system, with such fast formation kinetics, the progress of the reaction is difficult to monitor. The different images do reflect however, stages in the formation of an outer silver shell, beginning with coalescence of clusters (Figure 6a) and later the formation of a continuous shell.

Figure 7a displays absorption spectra of the Ag_2O precursor nanoparticles, of the hollow silver nanoparticles, and of silver nanoparticles formed by slower reduction with sodium ascorbate as the reducing agent. The hollow nanoparticles exhibit a plasmon resonance absorption peak at ~480 nm, while the slowly reduced sample, yielding a variety of nanoparticle shapes and aggregates (as in Figure 5a) produced a typical spherical nanoparticle plasmon resonance peak at ~400 nm with a large red-shifted tail due to the aggregates and non-spherical shapes. The plasmon resonance frequency of the shells is red-shifted as expected.[21] Xia and co-workers used a discrete dipole approximation (DDA) calculation to estimate the plasmonic response of similar hollow Ag particles[22] of 40 nm outer diameter and 5 or 10 nm thick shell. The calculated spectra were similar to Figure 7a. The 480 nm peak wavelength in the present work, where average shell thickness is 7 nm, is red-shifted relative to the peak calculated for the 10 nm shell thickness (~440 nm) and blue-shifted relative to the 5 nm shell (~540 nm).

Figure 7b displays a series of spectra acquired during the first second of nanoparticle formation after the addition of the borohydride. It can be seen that at time zero the spectrum is that of the Ag_2O and that after about 600 ms the reaction is

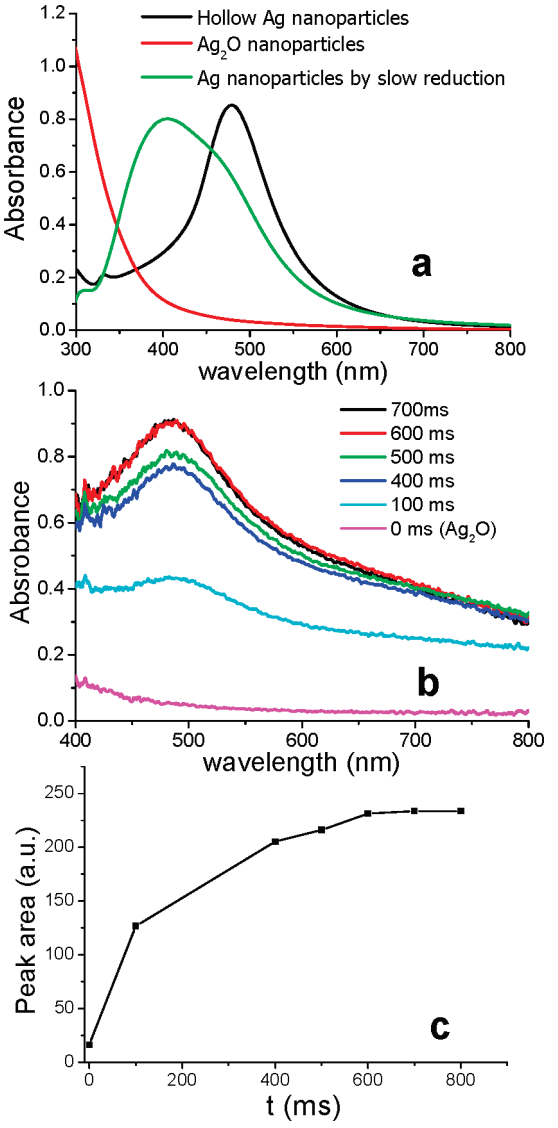

Figure 7. (**a**) Absorption spectra of three different samples: original Ag_2O nanoparticles (red), hollow silver nanoparticles (black), and regular nanoparticles and aggregates formed by slow reduction (green). (**b**) Time evolution of the absorption at the first 700 ms of the reaction. At time zero the spectrum corresponds to Ag_2O nanoparticles. (**c**) Time evolution of the integrated area under the plasmon absorption peak.

completed. A rough estimate for the amount of reduced silver can be obtained by integrating the plasmon absorption peak at each spectrum. The baseline shifted up at preliminary reduction stages because of light scattering by the evolving hydrogen bubbles. Figure 7c displays a plot of this integral as a function of time. A rough exponential fit to this curve yielded a reaction time constant of ~130 ms.

The formation of single crystal shells in such a fast, kinetically controlled process is difficult to explain. The reduction initiates in many nucleation centers around the Ag_2O cores, as seen in Figure 6a and thus the growth of a single crystalline shell is very surprising . Recently, it has been shown by Alivisatos and coworkers that for hollow ZnS nanoparticles formation via the Kirkendall effect[23] the obtained particles preserve the morphology of the template oxide particles. In addition, Tang and

dx.doi.org/10.1021/cm102991z |*Chem. Mater.* 2011, 23, 1239–1245

Ouyang have demonstrated the formation of single crystal silver selenide hollow nanoparticles in the oxidation of silver nanoparticles with selenium.[24] The reaction presented here is somewhat different, since reduction is taking place and not anion exchange or metal oxidation. We believe that the mechanism is somewhat similar to that proposed by Yang et al.[19] Shortly, a first layer of silver is deposited (supported by the images taken after partial reduction, Figure 6a) followed by further counter diffusion of reducing species (and/or electrons transferred from the reducing agent through the silver) and silver cations at different rates. Counter-diffusion might proceed in solid state or more likely, in light of the fast kinetics and moderate solubility of the core material, through solution phase, moving through gaps in the formed shell. Surface diffusion along the pores formed in the shell may occur as well, but it is believed that the solution phase diffusion is the main transport mechanism. The latter was previously described as a possible mechanism in Kirkendall type processes.[18d] The difference between the rates of electron transfer/diffusion would affect the outcome of the process. In the simple reduction process it was observed that BH_4^- species can diffuse or transfer electrons quite efficiently, as proven by the formation of hollow nanoparticles with cavity size smaller than the original template nanoparticle. However, when larger species are involved, such as other reducing agents or sulfide and bromide anions, the reaction probably proceeds mainly through diffusion of silver cations. An anion exchange with sulfide ions also forms hollow morphologies, but probably it involves mainly outward diffusion of the silver cations.[23]

The issue of charge balance in the transforming nanoparticles is also an important consideration. While certain transformations, such as oxidation of metals, are charge balanced;[17,24] others, like anion exchange[23] or the present case, must involve some mechanism to transport positive charges into the core of the nanoparticle. The simplest mechanism to accommodate this requirement is through solution phase diffusion of reducing agent, as well as counterions into the dissolving core, rather than complex solid inward diffusion of various species through the shell.

The reported hollow Ag nanoparticles are metastable, as probably expected from such structures, especially if the inner surface is not well stabilized. These hollow nanoparticles collapse to a compact cluster of smaller nanoparticles on the scale of ~10 days (Supporting Information, Figure S5).

CONCLUSION

In summary, we have demonstrated a new nanoscale transformation reaction that produces single crystal hollow silver nanospheres. This effect resembles the nanoscale Kirkendall effect, in the sense that it is a counter diffusion process, with the exception that the inward diffusion rate is probably very fast in the present work. Silver oxide, in this context proves to be an interesting material for transformation reactions, probably because of an exceptionally high cation diffusion rate, and perhaps also because of its moderate solubility. The technique could be extended to other materials via controlled core material solubility and ions diffusion rates, and diffusion efficiency of the reacting species into the template crystal. This may lead to synthesis of a large variety of hollow metal nanostructures, with varying compositions and shapes. One interesting potential application of the silver nanoshells is for near-field enhancement of Raman scattering which was predicted to be particularly large for hollow nanoparticles.[21] Special interests also involve the single crystalline nature of these nanoparticles, since it was previously demonstrated that electronic and optical properties are governed by crystallinity. In particular, single crystalline particles should produce relatively narrow surface plasmon resonances because of reduced scattering.[24]

ASSOCIATED CONTENT

Supporting Information. TEM images of additional samples and XPS results. This material is available free of charge via the Internet at http://pubs.acs.org.

AUTHOR INFORMATION

Corresponding Author
*E-mail: gilmar@post.tau.ac.il.

ACKNOWLEDGMENT

A.B.M. thanks the Tel Aviv University Center for Nanoscience and nanotechnology for a scholarship. This work is funded by the ISF Converging Technologies program Grant 1714/07. The authors are grateful to Dr. Larisa Burstein for the XPS measurements, to Dr. Zahava Barkai for the SEM images, and to Prof. Diana Golodnitsky for critical reading of the manuscript.

REFERENCES

(1) Zhou, H. S.; Honma, I.; Komiyama, H.; Haus, J. W. *Phys. Rev. B.* **1994**, *50*, 12052–12056.
(2) (a) Averitt, R. D.; Sarkar, D.; Halas, N. J. *Phys. Rev. Lett.* **1997**, *78*, 4217–4220. (b) Oldenburg, S. J.; Averitt, R. D.; Westcott, S. L.; Halas, N. J. *Chem. Phys. Lett.* **1998**, *288*, 243–247.
(3) Jackson, J. B.; Halas, N. J. *J. Phys. Chem. B* **2001**, *105*, 2743–2746.
(4) (a) Oldenburg, S. J.; Westcott, S. L.; Averitt, R. D.; Halas, N. J. *J. Chem. Phys.* **1999**, *111*, 4729–4735. (b) Jackson, J. B.; Halas, N. J. *Proc. Natl. Acad. Sci. U.S.A.* **2004**, *101*, 17930–17935. (c) Lal, S.; Grady, N. K.; Kundu, J.; Levin, C. S.; Lassiter, J. B.; Halas, N. J. *Chem. Soc. Rev.* **2008**, *37*, 898–911.
(5) Zhang, P.; Guo, Y. *J. Am. Chem. Soc.* **2009**, *131*, 3808–3809.
(6) Acevedo, R.; Lombardini, R.; Halas, N. J.; Johnson, B. R. *J. Phys. Chem. A* **2009**, *113*, 13173–13183.
(7) (a) Le, F.; Brandl, D. W.; Urzhumuv, Y. A.; Wang, H.; Kundu, J.; Halas, N. J.; Aizpurua, J.; Nordlander, P. *ACS Nano* **2008**, *2*, 707–718. (b) Kundu, J.; Le, F.; Nordlander, P.; Halas, N. J. *Chem. Phys. Lett.* **2008**, *452*, 115–119.
(8) Bardhan, R.; Grady, N. K.; Halas, N. J. *Small* **2008**, *4*, 1716–1722.
(9) Park, J.; Estrada, A.; Sharp, K.; Sang, K.; Schwartz, J. A.; Smith, D. K.; Coleman, C.; Payne, J. D.; Korgel, B. A.; Dunn, A. K.; Tunnell, J. W. *Opt. Express* **2008**, *16*, 1590–1599.
(10) (a) Hirsch, L. R.; Stafford, R. J.; Bankson, J. A.; Sershen, S. R.; Rivera, B.; Price, R. E.; Hazle, J. D.; Halas, N. J.; West, J. L. *Proc. Natl. Acad. Sci. U.S.A.* **2003**, *100*, 13549–13554. (b) Gobin, A. M.; Lee, M. H.; Halas, N. J.; James, W. D.; Drezek, R. A.; West, J. L. *Nano Lett.* **2007**, *7*, 1929–1934. (c) Zhang, J. Z. *J. Phys. Chem. Lett.* **2010**, *1*, 686–695.
(11) (a) Kim, S. W.; Kim, M.; Lee, W. Y.; Hyeon, T. *J. Am. Chem. Soc.* **2002**, *124*, 7642–7643. (b) Jana, S.; Ghosh, S. K.; Nath, S.; Pande, S.; Praharaj, S.; Panigrahi, S.; Basu, S.; Endo, T.; Pal, T. *Appl. Catal., A* **2006**, *313*, 41–48.
(12) Sun, Y.; Xia, Y. *Anal. Chem.* **2002**, *74*, 5297–5305.
(13) (a) Caruso, F.; Spasova, M.; Maceira, V. S.; Liz-Marzán, L. M. *Adv. Mater.* **2001**, *13*, 1090–1094. (b) Cassagneau, T.; Caruso, F. *Adv. Mater.* **2002**, *14*, 732–736.
(14) (a) Sun, Y.; Xia, Y. *Science* **2002**, *298*, 2176–2179. (b) Sun, Y.; Mayers, B.; Xia, Y. *Adv. Mater.* **2003**, *15*, 641–646. (c) Sun, Y.; Xia., Y. *Nano Lett.* **2003**, *3*, 1569–1572.

(15) (a) Kirkendall, E. O. *Trans AIME* **1942**, *147*, 104. (b) Smigelskas, A. D.; Kirkendall, E. O. *Trans AIME* **1947**, *171*, 130.
(16) Schröder, H.; Samwer, K.; Köster, U. *Phys. Rev. Lett.* **1985**, *54*, 197–200.
(17) Yin, Y.; Rioux, R. M.; Erdonmez, C. K.; Hughes, S.; Somorjai, G. A.; Alivisatos, A. P. *Science* **2004**, *304*, 711–714.
(18) (a) Li, Q.; Penner, R. M. *Nano Lett.* **2005**, *5*, 1720–1725. (b) Fan, H. J.; Knez, M.; Scholz, R.; Nielsch, K.; Pippel, E.; Hesse, D.; Zacharias, M.; Gösele, U. *Nat. Mater.* **2006**, *5*, 627–631. (c) Cabot, A.; Puntes, V. F.; Shevchenko, E.; Yin, Y.; Balcells, L.; Marcus, M. A.; Hughes, S. M.; Alivisatos, A. P. *J. Am. Chem. Soc.* **2007**, *129*, 10358–10360. (d) Fan, H. J.; Gösele, U.; Zacharias, M. *Small* **2007**, *3*, 1660–1671.
(19) Yang, J.; Qi, L.; Lu, C.; Ma, J.; Cheng, H. *Angew. Chem., Int. Ed.* **2005**, *44*, 598–603.
(20) Nam, K. M.; Shim, J. H.; Ki, H.; Choi, S. I.; Lee, G.; Jang, J. K.; Jo, Y.; Jung, M. H.; Song, H.; Park, J. T. *Angew. Chem., Int. Ed.* **2008**, *47*, 9504–9508.
(21) Hao, E.; Li, S.; Bailey, R. C.; Zou, S.; Schatz, G. C.; Hupp, J. T. *J. Phys. Chem. B* **2004**, *108*, 1224–1229.
(22) Wiley, B. J.; Im, S. H.; Li, Z. Y.; McLellan, J.; Siekkinen, A.; Xia, Y. *J. Phys. Chem. B* **2006**, *110*, 15666–15675.
(23) Park, J.; Zheng, H.; Jun, Y. W.; Alivisatos, A. P. *J. Am. Chem. Soc.* **2009**, *131*, 13943–13945.
(24) Tang, Y.; Ouyang, M. *Nat. Mater.* **2007**, *6*, 754–759.